

Simulating Ultrasound Reflections Using Rayleigh Integral Method in Complex Biological Media

Malak Nasser¹, Walid Hassan^{1, 2}, Ali Hage-Diab¹ and Souheil Hakeem³

1. Department of Biomedical Engineering, Lebanese International University, Moseitbeh, Beirut 146404, Lebanon

2. Department of Biomedical Physics, Lebanese University, Hadath, Beirut 657314, Lebanon

3. Biomedical Research Department, Sonopaths, Sparta, NJ 07871, USA

Received: July 22, 2013 / Accepted: October 22, 2013 / Published: December 30, 2013.

Abstract: This paper exploits the Rayleigh integral method to simulate the propagation of transmitted ultrasonic waves and received echoes through various media. Performed simulations study the effect of apodization using different types of windows and the effect of medium properties on the reflections obtained. All estimations are done using the Rayleigh integral method simplified by the Fresnel approximation. Five different interfaces are considered: tissue-bone-tissue, tissue-fat-bone, fat-muscle-bone, air-fat-bone and water-fat-bone. The apodization simulations show that the hamming window is more efficient than the rectangular and triangular windows for obtaining a more consistent beam. In the second set of simulations, reflections are mapped with respect to the depth from which these reflections are generated. It demonstrates that the solid and water media allow for the attainment of echoes from deeper regions as compared to the air medium. Matlab is used as the simulation framework.

Key words: Ultrasound, reflections, Rayleigh integral, apodization.

1. Introduction

The boundary elements method has been used to predict radiated sound from different structures in a complex biologic medium. Over the years, some approximations to the boundary integral equation have been suggested to solve problems faced with the conventional boundary element method. The most common approximations are based on the Rayleigh integral technique [1]. The Rayleigh integral method was developed over a century ago by Rayleigh [2]. It provides a simple but exact representation for the sound radiation from a flat vibrating surface mounted on an infinite rigid baffle. Several studies reported many advantages of the Rayleigh integral method over the boundary element method such as the ability to compute 3-D radiation and acoustic quantities in a fraction of the time, the speed of calculation, the few

computer resources that are needed, the ease of implementation since it does not require a system of equations, and the reliability of results without the disadvantage of creating and inverting large system matrices [1, 3]. Rayleigh waves have been studied and applied to many applications for different purposes. One study performed by W. Veronesi and W. Hassan in 2003 focused on the behavior of the reflection coefficient of the Rayleigh wave from the interaction of surface acoustic waves with finite-size, surface breaking, semi-circular cracks. This was studied in the far field of the crack and when the depth of the crack was comparable to the wavelength of the interrogating surface wave [4].

In 2006, a model was developed by Dixon et al. for the prediction of the transient displacement of a Rayleigh wave generated by an electromagnetic acoustic transducer, operating on the Lorentz principle. Their study revealed that the orientation of the external magnetic field must be correct to achieve an efficient

Corresponding author: Walid Hassan, Ph.D., associate professor, research field: biomedical engineering. E-mail: walid.hassan@liu.edu.lb.

generation of the Rayleigh wave [5]. One of the most popular programs for mapping ultrasonic field is the field program that was developed by Jensen et al. in 1992 [6]. This program underwent several enhancements since its first version. In 2009, a new simulation program was developed by Moraru et al., which like the Field program allowed the simulation of different types of ultrasound transducers. In addition, it allowed the control of both, the focusing and the apodization of the transducer dynamically, making it possible to simulate various types of ultrasound imaging systems. As opposed to the field program, an improved simulation method for calculating the ultrasound field of arrays, based on the Rayleigh integral instead of the Tupholme-Stepanishen method, was integrated in this program. This method is more accurate, in which the result for a transducer element in an array is calculated and shifted to obtain the arising field from the remaining elements. The overall field resulting from an array is obtained by adding the fields generated from each individual transducer. In this program, the user could specify the array parameters including number and size of used elements, transducer's shape, frequency, excitation amplitude and propagating medium properties related to sound velocity and density. This flexibility in setting parameters allowed one to evaluate the effects of every parameter in the 2-D arrays field. The Rayleigh integral method was considered to be useful and of good accuracy in the cases where the desired tissue to be imaged was very close to the transducer, as in the case of intravascular sonography or low depth imaging, and it applied to both near-field and far-field [7]. Although the Field II program showed good efficiency on the imaging evaluation of single-element or linear array transducers, it met difficulties in analyzing annular structures. An alternative algorithm to the spatial impulse response method based on the direct solution of the Rayleigh integral was developed by Harrissa et al. in 2012 to evaluate the imaging pattern of annular ultrasonic transducer arrays with good

efficiency and accuracy [8]. In a later study applied by Goueygou et al. in 2012, the relationship between Rayleigh wave velocity at ultrasonic frequencies and capillary porosity was investigated in dry and various water saturations [9]. As expected, a linear decrease of Rayleigh wave velocity vs. porosity was observed for the intermediate saturation states, but not for the fully saturated and dry states. The Rayleigh integral method also serves purposes beyond the medical imaging domain. One example is its role in a strategy based on the one-way Rayleigh integral for the prediction and elimination/attenuation of ocean-bottom multiple energy on synthetic marine seismic data [10]. However, in the overall mentioned works, the apodization in complex medium such as biologic tissues was less considered. The basic reflections in a scattering medium such as bone using Rayleigh integral technique with apodization constituted the core of this study.

2. Materials and Methods

The Rayleigh integral is basically a statement of Huygens' principle that the field is found by summing the contributions of all the infinitely small area elements that make up the aperture [11]. The field of a point source of small dimensions gives spheres whose diameters increase at further distances (Fig. 1).

According to Huygen's diffracting principle, the pressure of a single spherical point source (Fig. 1) is given by Eq. (1) [13].

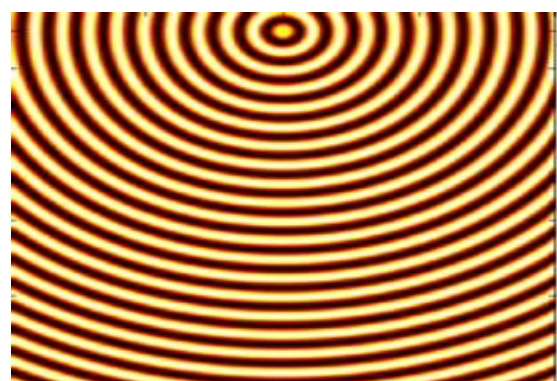


Fig. 1 Diffracting principle of a single spherical point source (taken from Ref. [12]).

$$P(r, \omega) = \frac{e^{i[\omega t - k|r - r_0|]}}{|r - r_0|} \quad (1)$$

where, ω is the angular frequency, t is the time, k is the wave number, r_0 is the distance from the center of the transducer surface to the transducer point, r is the distance from the center of the transducer surface to the field point, $|r - r_0|$ is the distance between the transducer and the field point, and $i = \sqrt{-1}$.

When increasing the number of point sources, the diffracting pattern (Fig. 2) is obtained by adding the contributions of all the point sources at specific field points.

The diffraction pattern is then presented as a summation of the pressure from all sources [13]:

$$P(r, \omega) = \sum_{n=1}^N \frac{e^{i[\omega t - k|r - r_0|]}}{|r - r_0|} \quad (2)$$

where, N is the number of sources used.

To simplify the implementation of the Rayleigh integral method, the Fresnel approximation can help in estimating the distance $|r - r_0|$ from the transducer to the field point.

$$|r - r_0| = \sqrt{(x - x_0)^2 + (y - y_0)^2 + z^2} \quad (3)$$

The equations above were used to simulate the ultrasound field pattern resulting from different configurations using the Rayleigh integral method.

When mapping the ultrasonic beams some small beams of reduced intensity usually exist at the angle of the primary beam. These beams that are referred to as "sidelobes" would seem to be a false echo creating artifacts near the transducer. The amplitude of sidelobes is suppressed by exciting the outer elements in a manner less than those in the center, as shown in (Fig. 3), in a process known as "apodization" [14]. Reduce the sidelobes results in a broader mainlobe, and thus get a more consistent beam [15].

During apodization each sub-aperture is windowed and weighed by a different value. Some of the window functions used are: the rectangular amplitude window, the triangular amplitude window and the hamming amplitude window. Due to the importance of apodization, some simulations were first done to study the efficiency of each of the mentioned windows and

subsequently choose the most suitable one. After that, simulations were performed as shown in Fig. 4 starting by defining the used transducer and the type of excitation. In order to study the reflections obtained, different structures are defined. These structures are composed of different media, each defined by its acoustic impedance. All scenarios are shown in Figs. 5-9.

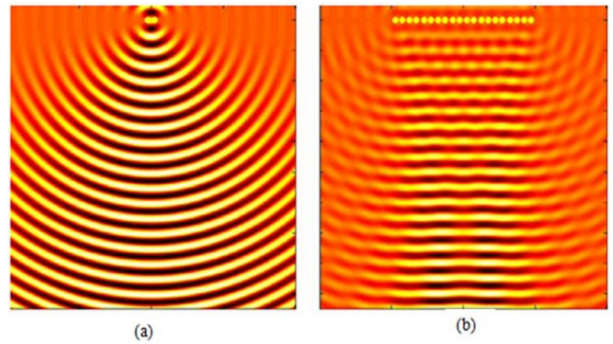


Fig. 2 Contribution of various point sources on the field. (a) 2 point sources; (b) several point sources (taken from Ref. [12]).

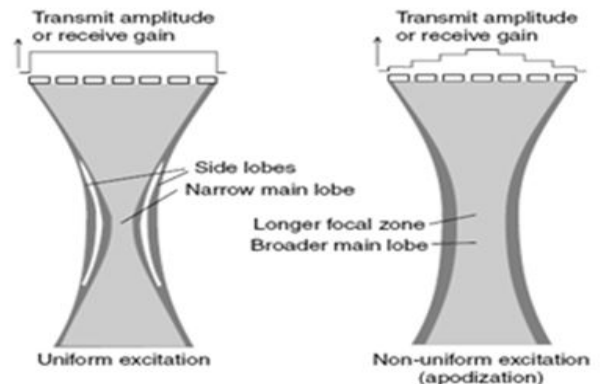


Fig. 3 Apodization (taken from Ref. [14]).

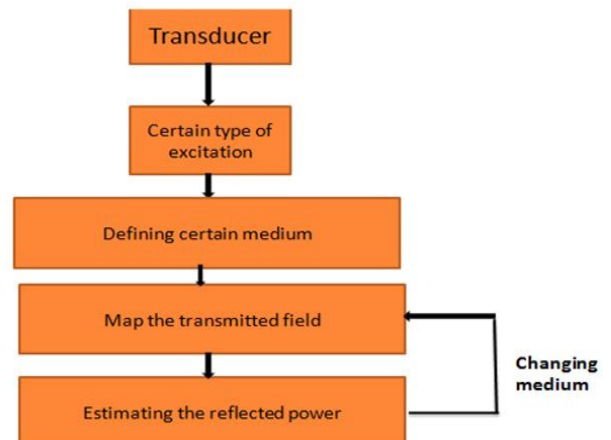


Fig. 4 Flowchart of the methodology.

Case 1: Tissue/bone/tissue interface (Fig. 5).



Fig. 5 Tissue/bone/tissue interface.

Case 2: Tissue/fat/bone interface (Fig. 6).



Fig. 6 Tissue/fat/bone interface.

Case 3: Fat/muscle/bone interface (Fig. 7).



Fig. 7 Fat/muscle/bone interface (taken from Ref. [16]).

Case 4: Air/fat/bone interface (Fig. 8).



Fig. 8 Air/fat/bone interface.

Case 5: Water/fat/bone interface (Fig. 9).



Fig. 9 Water/fat/bone interface.

The media used are: soft tissues, fat, muscle, air, water and bone. The following five different structures are considered.

3. Simulations

Simulations using the Rayleigh integral are first performed to study the effect of apodization by

defining a medium of biological tissues. Then the interfaces mentioned above are considered to map the reflected pressure as a function of depth. In this simulation, the field is mapped in the plane (xz) which is considered to be a matrix of points, each with specific coordinates (x, z). The response of each individual sub-aperture to each field point (f_p) (x, z) is estimated and then the overall field is considered to be the summation of them all. The aperture used falls in the (xz) plane and is parallel to the x-axis. The coordinates ($x_0, 0, z_0$) correspond to the location of sp (source point) on the line transducer used. Fig. 10 shows a simplified illustration of the geometry used.

A Matlab implementation is performed as shown in the flowchart of Fig. 11.

4. Results and Discussion

Before applying apodization, the field is mapped as a reference to study the effect of apodization later.

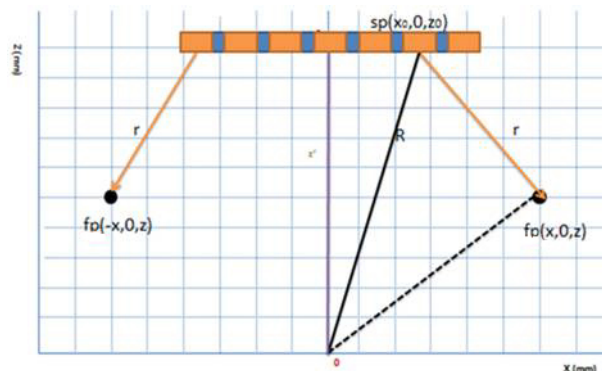


Fig. 10 Geometric presentation of the line transducer used.

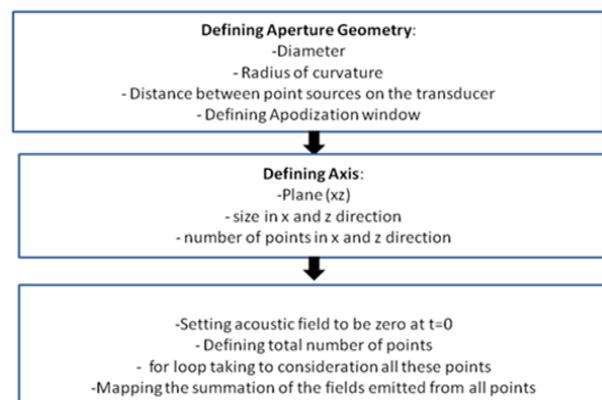


Fig. 11 Flowchart of steps followed in Matlab implementation.

When analyzing the obtained field in Fig. 12, sidelobes generated at the sides of the beam are well noticed. The existences of these artifacts affect the consistency of the main beam.

The results obtained using rectangular, triangular, and hamming windows are shown in Figs. 13-15, respectively.

Analyses of Figs. 13-15 indicate that the result of apodization differs based on the type of window used. In the case of the rectangular window, no changes in the field pattern are noticed. This result is expected due to the shape of the rectangular windows, where theoretically voltage of the same amplitude is applied to the transducers elements. Examining the results obtained from both, the triangular and hamming windows, a reduction in the sidelobes is realized. In these cases, due to the shapes of both windows, they offer the main concept of apodization. Using the triangular and hamming windows, transducer elements are weighed with different amplitudes. The highest one is applied to the central element, and then it is diminished from the center to the periphery, reducing the sidelobes. The sidelobes are reduced more in the case of the hamming window since the amplitude is reduced smoother than that in the triangular window. Reducing the sidelobes in both cases (triangular and hamming), leads to widening the main beam. From the obtained results, it is shown how adjusting the amplitude of the normal voltage across the aperture helps in reducing the sidelobes. This simulation shows that the hamming window is the most efficient choice to be used in the coming simulations.

4.1 Reflections Obtained

The ultrasound pressure generated by the source travels along an ultrasound beam, and the associated power is distributed across the beam. The power is mainly distributed evenly across the beam, but is more concentrated or intense near the center [17]. This is realized in the fields obtained using the Rayleigh integral method.

Several simulations beyond those listed in this paper were performed. The following results were noticed and helpful in analyzing and further understanding the colors of the bands obtained.

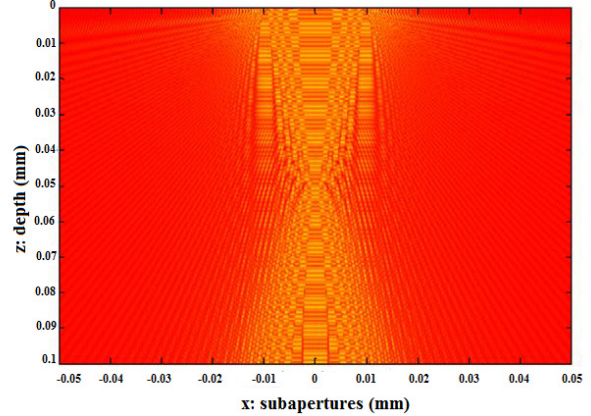


Fig. 12 Field obtained without apodization.

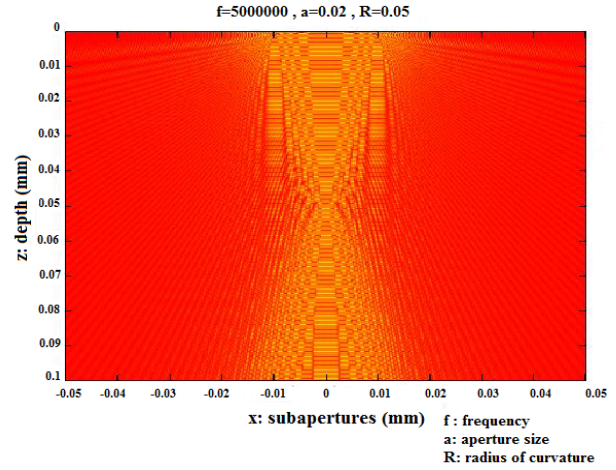


Fig. 13 Field obtained by apodizing using rectangular window.

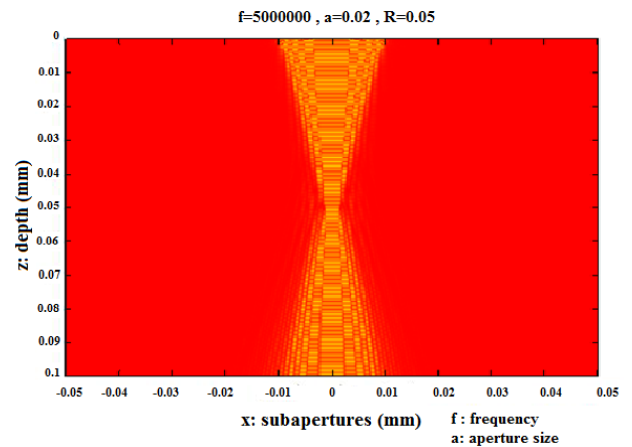


Fig. 14 Field obtained by apodizing using triangular window.

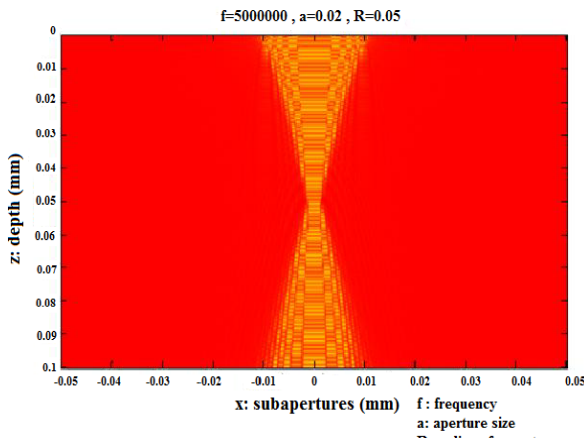


Fig. 15 Field obtained by apodizing using hamming window.

Comparing both the transmitted and the received waves in Fig. 16, it is realized that the highest variation in the pressure occurs in the second medium, which in this case is the bone medium. According to the values listed previously in Table 1, the wide, dark red bands indicate that a high pressure exists, mainly near the front and the back boundary of the bone medium, and this is due to the high difference between the acoustic impedance of bone, $Z_{bone} = 7.38 \times 10^6 \text{ kg/m}^2\text{s}$, and that of soft tissue, $Z_{tissue} = 1.62 \times 10^6 \text{ kg/m}^2\text{s}$. The pressure at the boundary reaches about 115 Pa. Within the bone structures, a series of dark red and dark blue bands, with equal widths, is obtained. This indicates that the ultrasound waves' propagation in the bone causes the medium to undergo compression followed by rarefaction. The maximum pressure reaches up to $1.7 \times 10^4 \text{ Pa}$, and the minimum pressure reaches $-1,622 \text{ Pa}$. If we are dealing with real bone medium, then this rapid activity of ultrasound waves could be due to the bone structure. Different densities are encountered within the bone causing the pressure to increase at one time and decrease at another, depending on the density faced. This complexity in the structure of the bone causes most of the ultrasound waves to be reflected or scattered. Low pressures, indicated by dark and light blue bands, are reflected from the soft tissues.

Since the acoustic impedance of soft tissue and fat are close to each other, low pressures are reflected at

Table 1 The range of pressure corresponding to each color of the pressure bands.

Pressure range (Pa)	Pressure band color
< 20	Dark blue
20-29	Light blue
30-36	Green
37-46	Yellow
47-56	Orange
57-60	Red
> 60	Dark red

the boundary between them, which is indicated by dark and light blue colors as shown in Fig. 17. At their boundary, the pressure is about 12 Pa. As ultrasonic waves continue to propagate, the pressure increases, due to several interactions taking place, and reaches about 160 Pa at depth = 0.028 mm. At depth = 0.04 mm, the point at which the ultrasound wave encounters the front boundary of the bone medium, and the pressure increases up to 6,819 Pa. The ultrasound at first meets the compact bone, which is very dense, thus a high pressure is reflected [18]. As the ultrasound propagates through the bone, most of the ultrasonic pressure is reflected. These reflections are of high pressures reaching $6.31 \times 10^4 \text{ Pa}$.

According to Fig. 18, at the point of interface between the fat medium and the muscle medium, a low pressure (about 0.5 Pa) is reflected since the difference between the acoustic impedances of the two are small, $Z_{fat} = 1.33 \times 10^6 \text{ kg/m}^2\text{s}$ and $Z_{muscle} = 1.74 \times 10^6 \text{ kg/m}^2\text{s}$. As the ultrasound continues its path within the muscle medium, due to its interaction with different tissues, the pressure increases to reach 116 Pa. Since the difference in the acoustic impedance between muscle and bone mediums is high, the pressure reflected at their interface is much higher and equals about 6,755 Pa. As it moves further within the bone medium and encounters the complex structure of bone with different densities, the pressure is reflected as a higher value, where it reaches a maximum of $6.3 \times 10^4 \text{ Pa}$. After that, it starts to decrease since no medium is faced after the bone medium, and the intensity of the ultrasonic wave decreases following further interactions.

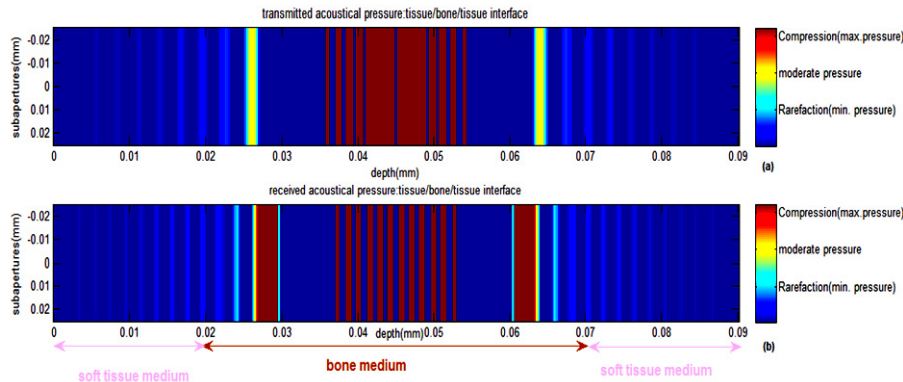


Fig. 16 Tissue-bone-tissue interface: (a) transmitted wave; (b) received wave.

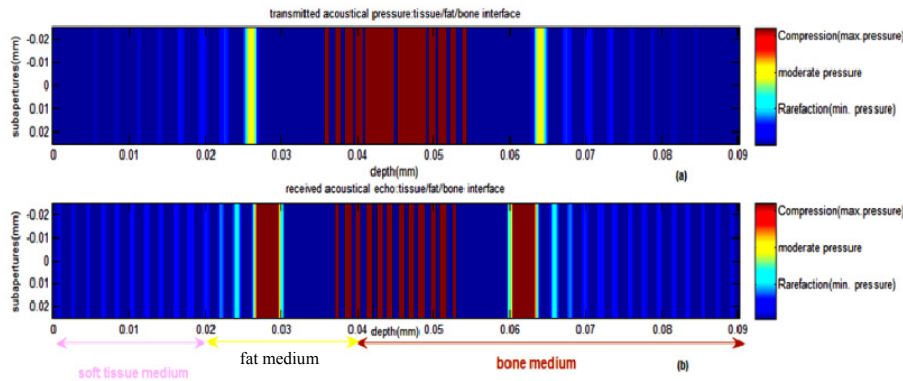


Fig. 17 Tissue-fat-bone interface: (a) transmitted wave; (b) received wave.

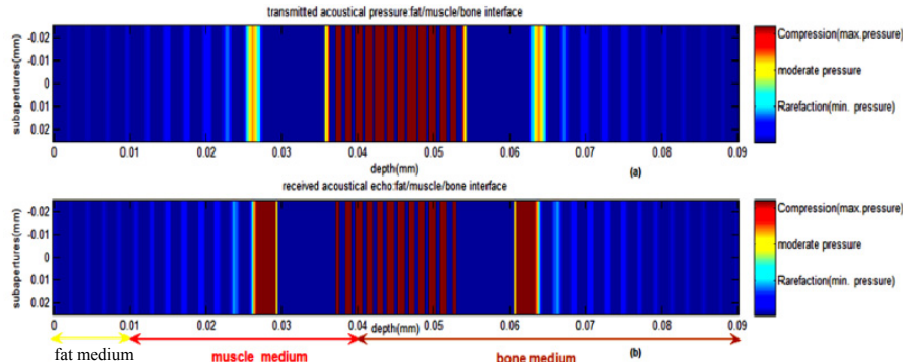


Fig. 18 Fat-muscle-bone interface: (a) transmitted wave; (b) received wave.

Air is known to be “ultrasound’s enemy” as it disperses most of the ultrasonic waves. This can be justified since the propagation of ultrasonic waves through different media depends mainly on the particles’ displacement in these media. The particles within an air or gas medium are distant from one another, unlike those in a water medium. The separation of the air’s particles does not aid the ultrasonic waves’ movement because each particle

fails to accelerate the next. Thus, the propagation of the ultrasonic waves is inhibited and the pressure is scattered. This simulation shows the sensitivity of a parameter other than the acoustic impedance. That parameter is the speed of sound in the medium, and has an effect on the results obtained by the Rayleigh integral method. Analyzing the Rayleigh integral equation given by Eq. (2), the term k that stands for the wave number depends on the speed of sound in the

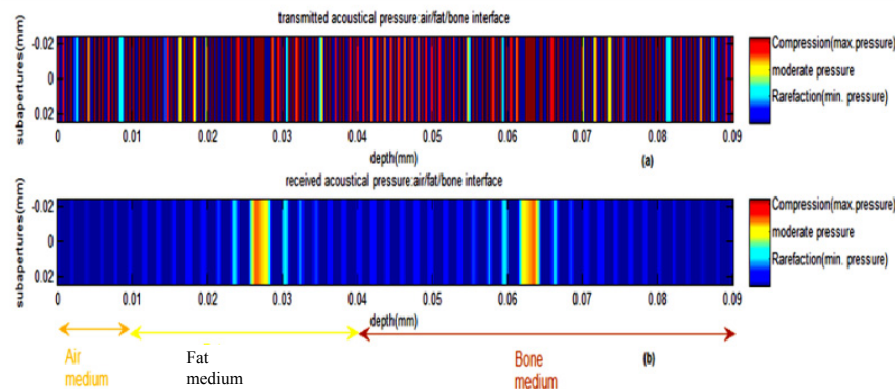


Fig. 19 Air-fat-bone: (a) transmitted pressure; (b) received pressure.

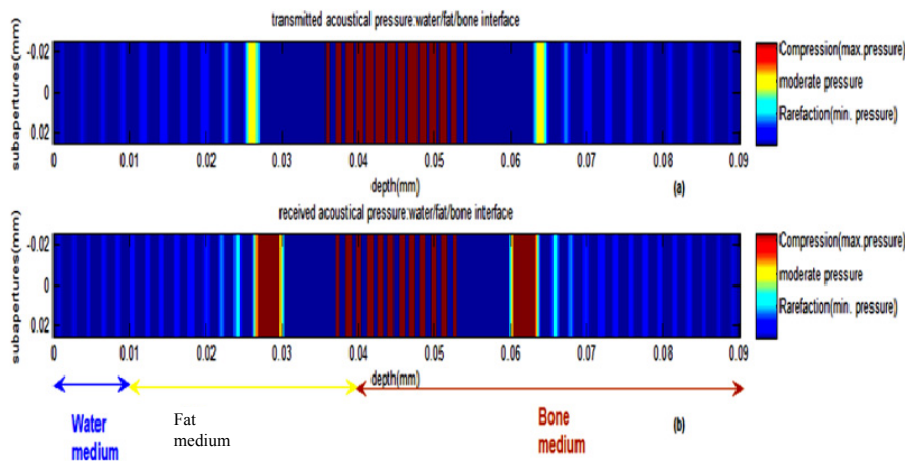


Fig. 20 Water-fat-bone: (a) transmitted pressure; (b) received pressure.

medium used. The first medium is considered to be the transmitted one, while the remaining two are the main sources of reflections. In Fig. 19, due to the low speed within the air medium, transmitted reflections are dispersed all over the beam. During reception, although the pressure is mainly focused in the center, fluctuations in its value are noticed. The maximum pressure reaches 394 Pa, which is small relative to the previous cases.

Solids and liquids consist of molecules held together by elastic forces connecting each molecule to its nearest neighbors. If one molecule is set in vibration, it will cause its immediate neighbors to vibrate, and in turn their neighbors, and so on until the vibration has propagated throughout the entire material. This is known as a wave. As stated previously, the results look similar to those in

previous cases in which bone interacts with soft tissue and fat as in Fig. 20. All these mediums: water, soft tissue, muscle and fat have close acoustic impedances. Acoustic impedance is the main factor that determines the percentage or amount of reflections. In addition, the values for the speed of sound in human soft tissues are rather similar. They are all within 5% of this average value, not much different from the value in water [17] $c_t = 1,540$ m/s, $c_f = 1,446$ m/s, $c_m = 1,626$ m/s and $c_w = 1,480$ m/s.

5. Conclusions

The existence of artifacts caused by the sidelobes affects the consistency of the main beam. Apodization works on improving the beam by reducing these sidelobes. Apodization can be applied using different types of windows. In this paper, the hamming window

was proven to be the most efficient one for the simulations performed. The Rayleigh integral method was used to study the propagation of ultrasonic waves, which primarily depends on the displacement of the particles within the encountered medium. Solid and water mediums allow the ultrasonic wave to propagate, whereas the air medium acts as a barrier and prohibits such propagation. The Rayleigh integral method is beneficial for studying reflections with respect to the depth of a given structure. In the Rayleigh integral, parameters other than the acoustic impedance can affect mapping of the reflected pressure, such as the speed of sound, causing it to be considered a more flexible method. This is contrary to the convolution method—to be compared to the Rayleigh integral method in a future study—where acoustic impedance is the main parameter in determining the amount of reflections.

References

[1] D.W. Herrin, A new look at the high frequency boundary element and Rayleigh integral approximations, Society of Automotive Engineers, Inc., 2003.

[2] J.W.S. Rayleigh, The Theory of Sound, 2nd ed., MacMillan, 1896, vol. II.

[3] P. Fiala, F. Augusztinovicsz, A. Kotseh, A.B. Nagy, Prediction of radiated noise in enclosures using a Rayleigh integral based technique, in: The 33 International Congress and Exposition on Noise Contr. & Engineering, Aug. 2004.

[4] W. Veronesi, W. Hassan, Finite element analysis of Rayleigh wave interaction with finite-size, surface-breaking cracks, United Technologies Research Center, USA, 2003, pp. 41-52.

[5] S. Dixon, K.T.V. Grattan, R.S. Edwards, X. Jian, A model for pulsed Rayleigh wave and optimal EMAT design, University of Warwick, City University, London, Sensors and Actuators A 128 (2006) 296-304.

[6] J.A. Jensen, N.B. Svendsen, Calculation of Pressure Fields from Arbitrarily Shaped, Apodized, and Excited Ultrasound Transducers, IEEE Transactions on Ultrasonics, Ferroelectrics, and Frequency Control, Mar. 1992, Vol. 39.

[7] L. Moraru, M.C. Nicolae, L. Onose, Simulation of acoustic fields from medical ultrasound transducers, Romanian J. Biophysics 19 (10) (2009) 277-283.

[8] N.R. Harrisa, Y. Qian, Direct Solution of the Rayleigh integral to obtain the radiation pattern of an annular array ultrasonic transducer, Procedia Engineering, XXVI 47 (9) (2012) 861-864.

[9] M. Goueygou, Z. Lafhaj, B. Piwakowski, F. Soltani, Relationship between ultrasonic Rayleigh wave propagation and capillary porosity in cement paste with variable water content, Ecole Centrale de Lille, France, NDT&E International 54 (2012) 75-83.

[10] M. Antonio, C. Santos, L. Landau, P.P. Ferreira, Characteristics of the free surface multiple attenuation using wave field extrapolation, in: AAPG International Conference and Exhibition, Rio de Janeiro, 2009.

[11] J.J. Arendt, S.I. Nikolov, K.L. Gammelmark, M.H. Pedersen, Synthetic aperture ultrasound imaging, Ultrasonics 44 (2006) 5-15.

[12] T. Bjastad, L. Lovstakken, Acoustic field from an ultrasound transducer, MEDT8012, Class Lecture, Department of Circulation and Medical Imaging, Norwegian University of Science and Technology, [Online], <http://www.ntnu.no>.

[13] T.L. Szabo, Diagnostic Ultrasound Imaging: Inside Out, Elsevier Academic Press, 2004, Ch. 6, pp. 140-142.

[14] K. Martin, T. Whittingham, Transducer and Beam-forming, in Diagnostic Ultrasound: Physics and Equipment, Cambridge University Press, New York, United States of America, 2010, Ch. 3, p. 31.

[15] T.L. Szabo, Diagnostic Ultrasound Imaging: Inside Out, Elsevier Academic Press, 2004, Ch. 6, pp. 148-149.

[16] C. Kwan, M. Gharibians, BodyMetrix Ultrasound Body Fat Measurement. Core Ten Physical Evolutions, [Online], <http://coreten.ca/wellness-services/body-fat-measurement/>.

[17] K. Martin, K. Ramnarine, “Physics” in Diagnostic Ultrasound: Physics and Equipment, Cambridge University Press, New York, United States of America, 2010, Ch. 2, pp. 8-10.

[18] P.M. Gauzellino, F.I. Zyberman, J.E. Santos, A study of ultrasonic wave propagation in bones, Latin American Applied Research 38 (4) (2008) 361-368.